51st AIAA Aerospace Sciences Meeting including the New Horizons Forum and Aerospace Exposition
07 - 10 January 2013, Grapevine (Dallas/Ft. Worth Region), Texas

AIAA 2013-0691

Comparison of SU/PG and DG Finite-Element Techniques for the Compressible Navier-Stokes Equations on Anisotropic Unstructured Meshes

Ryan S. Glasby[1]
Aerospace Testing Alliance, Arnold AFB, TN, 37388

Nicholas K. Burgess[1]
Science and Technology Corp., Moffet Field, CA 94035

W. Kyle Anderson[2]
SimCenter: National Center for Computational Engineering
University of Tennessee at Chattanooga, Chattanooga, TN 37403

Li Wang[1]
SimCenter: National Center for Computational Engineering
University of Tennessee at Chattanooga, Chattanooga, TN 37403

Dimitri J. Mavriplis[2]
Department of Mechanical Engineering, University of Wyoming, Laramie, WY 82071

Steven R. Allmaras[3]
Department of Aeronautics and Astronautics, Massachusetts Institute of Technology, Cambridge, MA 02139

In this paper computed results from Steamline Upwind/Petrov-Galerkin and Discontinuous Galerkin finite-element methods are compared for various two-dimensional compressible Navier-Stokes applications. Identical meshes are utilized for each comparison with linear, quadratic, and cubic elements employed. The order of accuracy is assessed for each scheme for viscous flows using the method of manufactured solutions, and results from each scheme are compared to experimental data. Each scheme is notionally of design order, and results from both compare well with experimental data. Both schemes are viable finite-element discretization techniques, and neither applies an unnecessary amount of artificial dissipation.

I. Introduction

THE continuing improvement of high-performance computers has recently led to renewed interest in higher-order finite-element (FE) techniques for compressible computational fluid dynamics (CFD) applications.[1-8] Finite-element techniques provide the capability of discretizing the flow field with arbitrarily shaped higher order elements, and they also allow for efficient grid spacing/polynomial order (h-p) refinement techniques. The utilization of a higher order finite-element scheme can generate a solution to the same level of accuracy as a first/second-order finite-volume scheme with substantially fewer degrees of freedom, potentially making such a scheme more computationally efficient.

Two of the most prevalent higher order finite-element techniques for the compressible Navier-Stokes equations are the Streamline Upwind/Petrov-Galerkin (SU/PG) and the Discontinuous Galerkin (DG) methods, and research efforts that utilize the DG method greatly outnumber those that utilize the SU/PG method. Each method attains

[1] AIAA Member
[2] AIAA Associate Fellow
[3] Senior Member AIAA

numerical stability for hyperbolic partial differential equations (PDEs) by spatially discretizing the governing equations with an upwind method. Upwinding is attained by modifying the central difference type Galerkin finite-element method. The SU/PG method employs upwinding by modifying the Galerkin weighting function,[9] and the DG method employs upwinding by separating adjacent elements and applying a flux jump condition that approximates a solution to the Riemann problem at the element interfaces.

For the current effort, quantitative and qualitative comparisons are conducted between the SU/PG and DG methodologies in an attempt to decipher the differences in error vs. measures of computational work on identical meshes. The method of manufactured solutions is applied to both methods to quantitatively describe the L2 norm of the discretization error vs. the number of degrees of freedom and the number of elements for a given mesh. Also, as a demonstration of each method's applicability to non-trivial geometries, each is implemented to generate a solution of the flow-field for the following cases using identical computational meshes: a steady-state NACA0012 airfoil at 1 deg. angle of attack (α) at a Mach number of 0.5 with a Reynolds number (Re) based on a chord length of 5,000, and a circular cylinder at a Mach number of 0.2 with a Reynolds number based on a diameter of 40. Linear, quadratic, and cubic elements are employed to discretize the field which means that the smooth portions of the solutions generated are notionally second-, third-, and fourth-order accurate. Both FE schemes use an exact (to machine precision including higher order contributions) Jacobian as an efficient and robust solver approach. Each FE scheme uses Newton's method to solve the non-linear set of equations which result from spatial and implicit temporal discretization. The inherent matrix systems are solved at each time-step with a preconditioned GMRES[10] method. The flow fields generated from each FE solver are qualitatively compared by evaluating various contours of variables of interest and quantitatively compared by evaluating force coefficients for the real-world problems with nontrivial geometries.

II. Governing Equations

The compressible Navier-Stokes (NS) equations in conservative form describe the conservation of mass, momentum, and total energy as follows:

$$\frac{\partial \boldsymbol{Q}(x,t)}{\partial t} + \nabla \cdot (\boldsymbol{F}(\boldsymbol{Q}) - \boldsymbol{F_v}(\boldsymbol{Q}, \nabla \boldsymbol{Q})) = 0 \quad \text{in} \quad \Omega \tag{1}$$

where Ω is a bounded domain. The vector of conserved flow variables, $\boldsymbol{Q}$, and the inviscid and viscous Cartesian flux vectors, $\boldsymbol{F}$ and $\boldsymbol{F_v}$ are shown in three spatial dimensions (even though the CFD solvers are currently two-dimensional [2-D]) as follows:

$$\boldsymbol{Q} = \begin{pmatrix} \rho \\ \rho u \\ \rho v \\ \rho w \\ E_t \end{pmatrix}, \qquad \boldsymbol{F}^x = \begin{pmatrix} \rho u \\ \rho u^2 + p \\ \rho uv \\ \rho uw \\ u(E_t + p) \end{pmatrix}, \qquad \boldsymbol{F}^y = \begin{pmatrix} \rho v \\ \rho uv \\ \rho v^2 + p \\ \rho vw \\ v(E_t + p) \end{pmatrix}, \qquad \boldsymbol{F}^z = \begin{pmatrix} \rho w \\ \rho uw \\ \rho vw \\ \rho w^2 + p \\ w(E_t + p) \end{pmatrix},$$

$$\boldsymbol{F}_v^x = \begin{pmatrix} 0 \\ \tau_{xx} \\ \tau_{xy} \\ \tau_{xz} \\ u\tau_{xx} + v\tau_{xy} + w\tau_{xz} + k\frac{\partial T}{\partial x} \end{pmatrix}, \quad \boldsymbol{F}_v^y = \begin{pmatrix} 0 \\ \tau_{yx} \\ \tau_{yy} \\ \tau_{yz} \\ u\tau_{yx} + v\tau_{yy} + w\tau_{yz} + k\frac{\partial T}{\partial y} \end{pmatrix}, \tag{2}$$

$$\boldsymbol{F}_v^z = \begin{pmatrix} 0 \\ \tau_{zx} \\ \tau_{zy} \\ \tau_{zz} \\ u\tau_{zx} + v\tau_{zy} + w\tau_{zz} + k\frac{\partial T}{\partial z} \end{pmatrix}$$

where ρ, p, and E_t denote the fluid density, pressure, and total energy per unit volume. $\boldsymbol{u} = (u, v, w)$ denotes the Cartesian velocity vector. τ is the fluid viscous stress tensor, and since the fluid is assumed to be Newtonian, τ is defined as

$$\tau_{ij} = \mu\left(\frac{\partial \boldsymbol{u}_i}{\partial \boldsymbol{x}_j} + \frac{\partial \boldsymbol{u}_j}{\partial \boldsymbol{x}_i} - \frac{2}{3}\frac{\partial \boldsymbol{u}_k}{\partial \boldsymbol{x}_k}\delta_{ij}\right) \tag{3}$$

where δ_{ij} is the Kronecker delta function, and the subscripts i, j, k, refer to the Cartesian coordinate components for $\boldsymbol{x} = (x, y, z)$. μ is the fluid dynamic viscosity obtained by Sutherland's law. p is the pressure, and for an ideal gas is defined by the equation of state as

$$p = (\gamma - 1)\left[E_t - \frac{1}{2}\rho(u^2 + v^2 + w^2)\right] \tag{4}$$

where γ is the ratio of specific heats and is 1.4 for air. k and T represent the thermal conductivity and temperature respectively.

III. Spatial Discretization

The computational domain Ω is divided into a set of nonoverlapping elements. Within each element the conserved flow variables are assumed to vary as the sum of a linear combination of the polynomial basis functions, $N(x, y, z)$, and the conserved flow variable at each node of the element, $\hat{Q}$ for the case where certain basis functions are employed as

$$\boldsymbol{Q}(x, y, z) = \sum_i \hat{Q}_i N_i(x, y, z) \tag{5}$$

The spatial discretization derivations for both the SU/PG and DG finite-element methods start with the weighted residual statement of the governing equations

$$\iiint_{\Omega_k} w_i \left[\frac{\partial \boldsymbol{Q}(\boldsymbol{x},t)}{\partial t} + \nabla \cdot (\boldsymbol{F}(\boldsymbol{Q}) - \boldsymbol{F}_{\boldsymbol{v}}(\boldsymbol{Q}, \nabla \boldsymbol{Q}))\right]_k \partial\Omega_k = 0 \tag{6}$$

The weighting function, w, for an element is defined as the sum of the linear combination of the polynomial basis functions and an arbitrary displacement, d. The weighting function for an element is defined as

$$w = \sum_i N_i(x, y, z) d_i \tag{7}$$

In order to implement the Galerkin method, the above weak form of the governing equations is integrated by parts as follows:

$$\iiint_{\Omega_k} w_i \frac{\partial \boldsymbol{Q}(\boldsymbol{x},t)}{\partial t} \partial\Omega_k - \iiint_{\Omega_k} \nabla w_i \cdot \big(\boldsymbol{F}(\boldsymbol{Q}) - \boldsymbol{F}_{\boldsymbol{v}}(\boldsymbol{Q})\big)\partial\Omega_k +$$

$$\iint_{\Gamma} w_i(\boldsymbol{F}(\boldsymbol{Q}) \cdot \boldsymbol{n} - \boldsymbol{F}_{\boldsymbol{v}}(\boldsymbol{Q}, \nabla \boldsymbol{Q}) \cdot \boldsymbol{n})\partial\Gamma = 0 \tag{8}$$

The Galerkin method is a central difference type method that is well-suited for elliptic PDEs, but is numerically unstable for convection dominated flows because the governing PDEs become strongly hyperbolic under these conditions. Upwinding is necessary to attain numerical stability for strongly hyperbolic PDE's. Upwinding can be applied by adding dissipation to a central difference type scheme. The SU/PG method incorporates upwinding by adding a term to the Galerkin weighting function that provides dissipation in the streamwise direction.[9] The DG method incorporates upwinding by separating adjacent elements and applying a flux jump condition that approximates a solution to the Riemann problem at element interfaces. The difference between the two methods is subtle. More precisely, the third term in Eq. (8) consists of the boundary contributions from all elements. Because the SU/PG method is continuous, the inter-element contributions vanish and only boundary terms are left. However, for the DG method the nodes that make up a face between adjacent elements are duplicated, and the number of degrees of freedom increases substantially compared to the SU/PG method for elements that have a substantial fraction of their nodes on the faces (lower order elements). Since upwinding is applied at the element interfaces for the DG method, the scheme is element-stable (with regards to solving the linear system). For the SU/PG method, upwinding is applied to each degree of freedom in a volumetric sense and the scheme is node-stable.

In order to derive the SU/PG method, the following integration is carried out for each element in the computational domain:

$$\iiint_{\Omega_k} w_i \frac{\partial \boldsymbol{Q}(\boldsymbol{x},t)}{\partial t} \partial\Omega_k - \iiint_{\Omega_k} \nabla w_i \cdot \big(\boldsymbol{F}(\boldsymbol{Q}) - \boldsymbol{F_v}(\boldsymbol{Q})\big) \partial\Omega_k +$$

$$\iiint_{\Omega_k} \left\{ \left(\frac{\partial w_i}{\partial x}[A] + \frac{\partial w_i}{\partial y}[B] + \frac{\partial w_i}{\partial z}[C] \right)[\tau] \left(\frac{\partial \boldsymbol{Q}(\boldsymbol{x},t)}{\partial t} + \nabla \cdot (\boldsymbol{F}(\boldsymbol{Q}) - \boldsymbol{F_v}(\boldsymbol{Q}, \nabla \boldsymbol{Q})) \right) \right\} \partial\Omega_k = 0 \tag{9}$$

In the above equation, $[A]$, $[B]$, and $[C]$ are the inviscid flux Jacobian matrices, and $[\tau]$ is a stabilization matrix that has the units of time. For inviscid flows, $[\tau]$ is defined as[11]

$$[\tau]^{-1} = \sum_i \left| \frac{\partial N_i}{\partial x}[A] + \frac{\partial N_i}{\partial y}[B] + \frac{\partial N_i}{\partial z}[C] \right| \tag{10}$$

$$\left| \frac{\partial N_i}{\partial x}[A] + \frac{\partial N_i}{\partial y}[B] + \frac{\partial N_i}{\partial z}[C] \right| = [T][|\Lambda|][T]^{-1} \tag{11}$$

where $[T]$ is the matrix of right eigenvectors and $[|\Lambda|]$ is the matrix of the absolute value of the eigenvalues of the left-hand side of Eq. (11). For viscous flows this definition of $[\tau]$ is overly dissipative and does not provide the design order of accuracy for viscous flows with low Reynolds numbers.[2] The following definition of $[\tau]$ is not overly dissipative for viscous flow with low Reynolds numbers and provides the design order of accuracy when verified with the method of manufactured solutions.[2] This is the L1 definition that is based on the L2 definition in Ref. (12).

$$[\tau]^{-1} = \sum_i \left(\left| \frac{\partial N_i}{\partial x}[A] + \frac{\partial N_i}{\partial y}[B] + \frac{\partial N_i}{\partial z}[C] \right| + \frac{\partial N_i}{\partial x_j}[K]_{jk} \frac{\partial N_i}{\partial x_k} \right) \tag{12}$$

In the above equation $[K]$ is the set of viscous flux Jacobian matrices.

In order to derive the DG method, the integration shown in Eq. (8) for the Galerkin method is carried out for each element in the computational domain, except that element basis functions that are discontinuous at the element interfaces are employed, and the fluxes present in the third term are modified. The inviscid flux, $\boldsymbol{F}(\boldsymbol{Q}) \cdot \boldsymbol{n}$, is now denoted as $\boldsymbol{F}^*(\boldsymbol{Q}) \cdot \boldsymbol{n}$ and is obtained as a solution of a local one-dimensional Riemann problem normal to the interface. The flux, $\boldsymbol{F}^*(\boldsymbol{Q}) \cdot \boldsymbol{n}$, depends on the internal interface state $\boldsymbol{Q}^-$ and the adjacent element interface state $\boldsymbol{Q}^+$as well as the orientation of the interface defined by the normal vector $\boldsymbol{n}$. Current implementations include the flux difference splitting schemes of Rusanov[13], Roe[14], HLL[15], and HLLC[16-18]. The viscous flux, $\boldsymbol{F_v}(\boldsymbol{Q}, \nabla \boldsymbol{Q}) \cdot \boldsymbol{n}$, is now denoted $\boldsymbol{F_v^*}(\boldsymbol{Q}, \nabla \boldsymbol{Q}) \cdot \boldsymbol{n}$ and is obtained via the symmetric interior penalty method (SIP)[19,20], which seeks to penalize the solution for being discontinuous at the element interfaces. The SIP numerical flux is given as

$$\boldsymbol{F_v}(\boldsymbol{Q}, \nabla \boldsymbol{Q}, w_i) \cdot \boldsymbol{n} = [\![w_i]\!]\{\boldsymbol{F_v}(\boldsymbol{Q}, \nabla \boldsymbol{Q})\} \cdot \boldsymbol{n} + [\![\boldsymbol{Q}]\!]\{\boldsymbol{F_v}(\boldsymbol{Q}, \nabla w_i)\} \cdot \boldsymbol{n} - \nu \{\boldsymbol{G}_{ij}\} [\![w_i]\!][\![\boldsymbol{Q}]\!] \tag{13}$$

where $\{*\}$ and $[\![*]\!]$ are the average and jump operators, respectively:

$$\{a\} = \frac{a^- + a^+}{2}, \quad [\![a]\!] = (a^- - a^+) \tag{14}$$

where a is a scalar, vector, or matrix and ν is the penalty parameter. The matrix $\boldsymbol{G}_{ij}$ is given such that

$$\begin{aligned} \boldsymbol{F}_v^x &= \boldsymbol{G}_{11} \frac{\partial \boldsymbol{Q}}{\partial x} + \boldsymbol{G}_{12} \frac{\partial \boldsymbol{Q}}{\partial y} + \boldsymbol{G}_{13} \frac{\partial \boldsymbol{Q}}{\partial z} \\ \boldsymbol{F}_v^y &= \boldsymbol{G}_{21} \frac{\partial \boldsymbol{Q}}{\partial x} + \boldsymbol{G}_{22} \frac{\partial \boldsymbol{Q}}{\partial y} + \boldsymbol{G}_{23} \frac{\partial \boldsymbol{Q}}{\partial z} \\ \boldsymbol{F}_v^z &= \boldsymbol{G}_{31} \frac{\partial \boldsymbol{Q}}{\partial x} + \boldsymbol{G}_{32} \frac{\partial \boldsymbol{Q}}{\partial y} + \boldsymbol{G}_{33} \frac{\partial \boldsymbol{Q}}{\partial z} \end{aligned} \tag{15}$$

IV. Numerical Results

A. Method of Manufactured Solutions

A quantitative study of the discretization error of both SU/PG and DG discretizations is conducted using the method of manufactured solutions (MMS), which applies a forcing term to the NS equations such that a known analytical solution satisfies the NS equations exactly. For this study, the exact solution of density, momentum, and total energy is specified at the boundary of the computational domain. The MMS nondimensional solutions for density, velocity, and total energy are shown in Fig. 1.

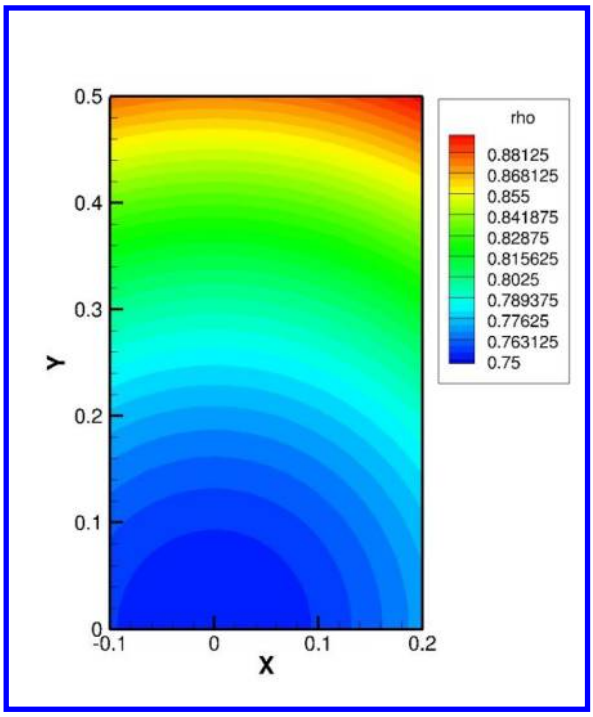

$$\rho = 0.5(\sin(x^2 + y^2) + 1.5)$$

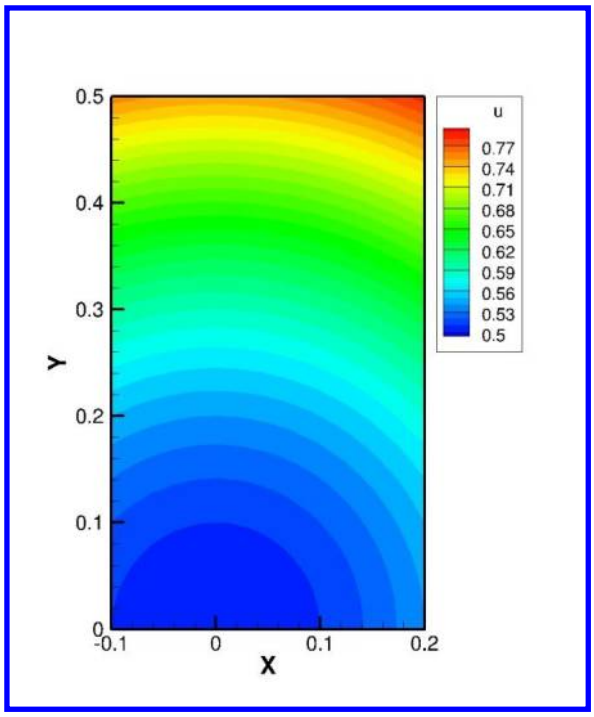

$$u = (\sin(x^2 + y^2) + 0.5)$$

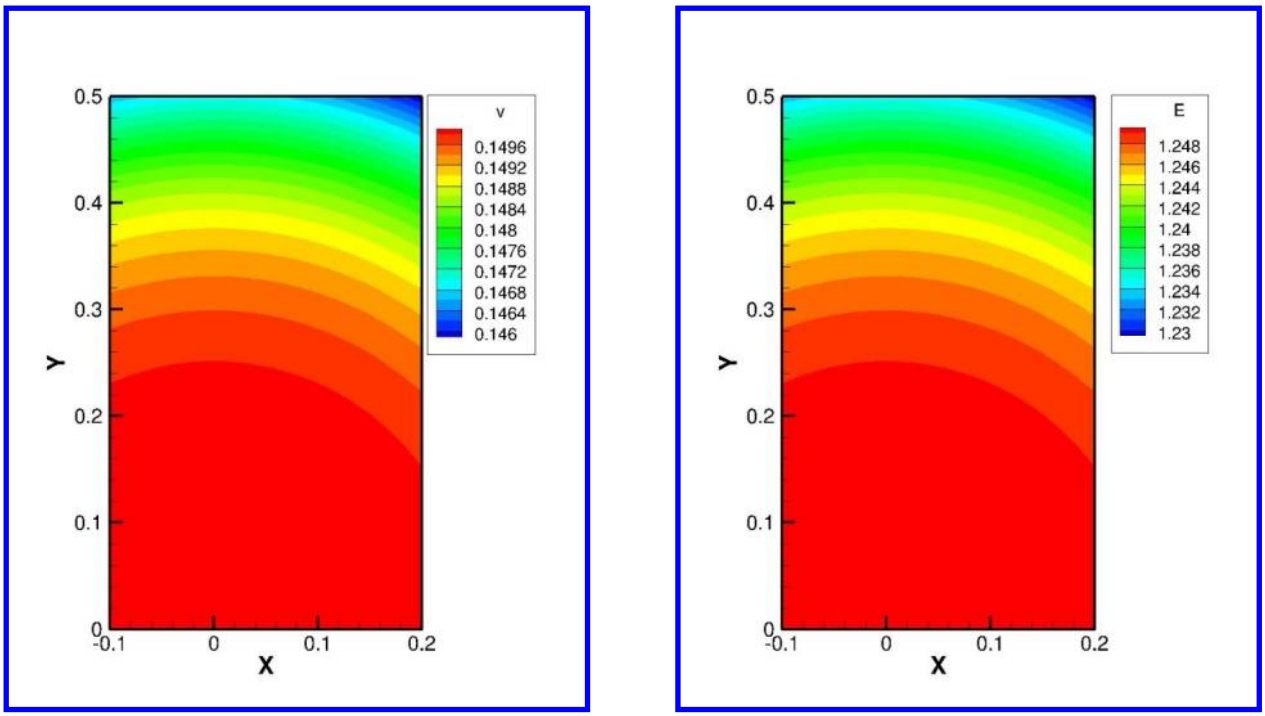

$$v = .1 * (\cos(x^2 + y^2) + 0.5) \qquad E_t = 0.5(\cos(x^2 + y^2) + 1.5)$$

Figure 1. Specified variable contours for the method of manufactured solutions.

The meshes utilized to conduct this study are a sequence of triangulated structured meshes with 90, 418, and 1,794 elements. All meshes have element aspect ratios of one. The three meshes are shown in Fig. 2.

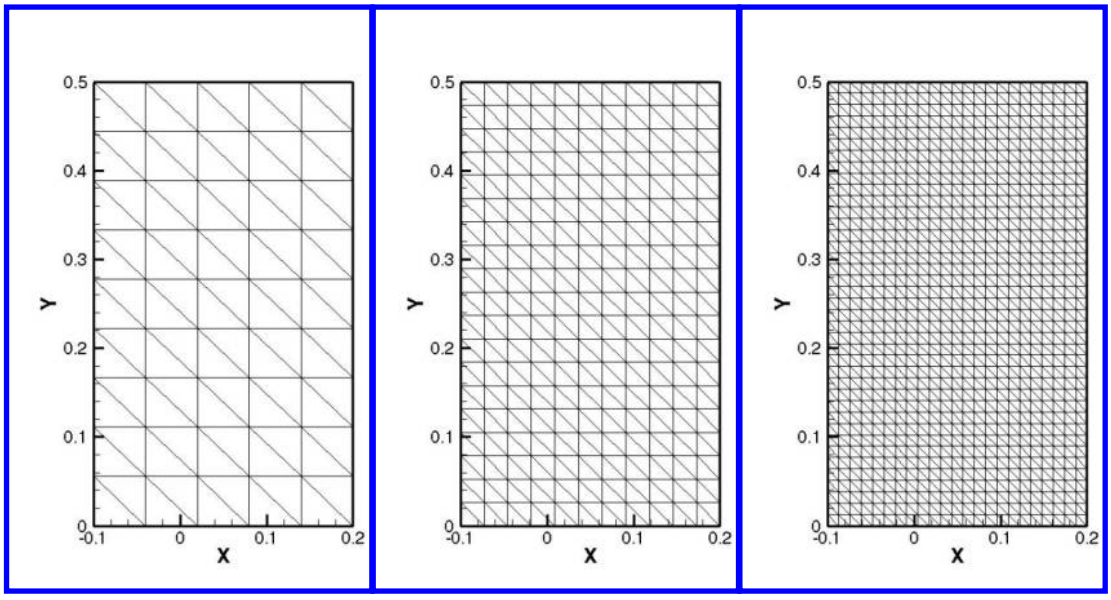

Figure 2. Meshes utilized for method of manufactured solutions study.

Fig. 3 shows the order of accuracy for the SU/PG and DG methods with linear, quadratic, and cubic (p = 1, 2, and 3) elements employed for a Reynolds number of 10 to be notionally of design order (order = 2 for linear elements, order = 3 for quadratic elements, and order = 4 for cubic elements). Figure 3 also shows that for a given level of error in density, velocity, or total energy, fewer degrees of freedom (N_{DoF}) are employed for the SU/PG

method as compared to the DG method for p = 1, 2, and 3. It should be noted that the solution with cubic elements for the DG method on the finest grid is outside of the asymptotic region.

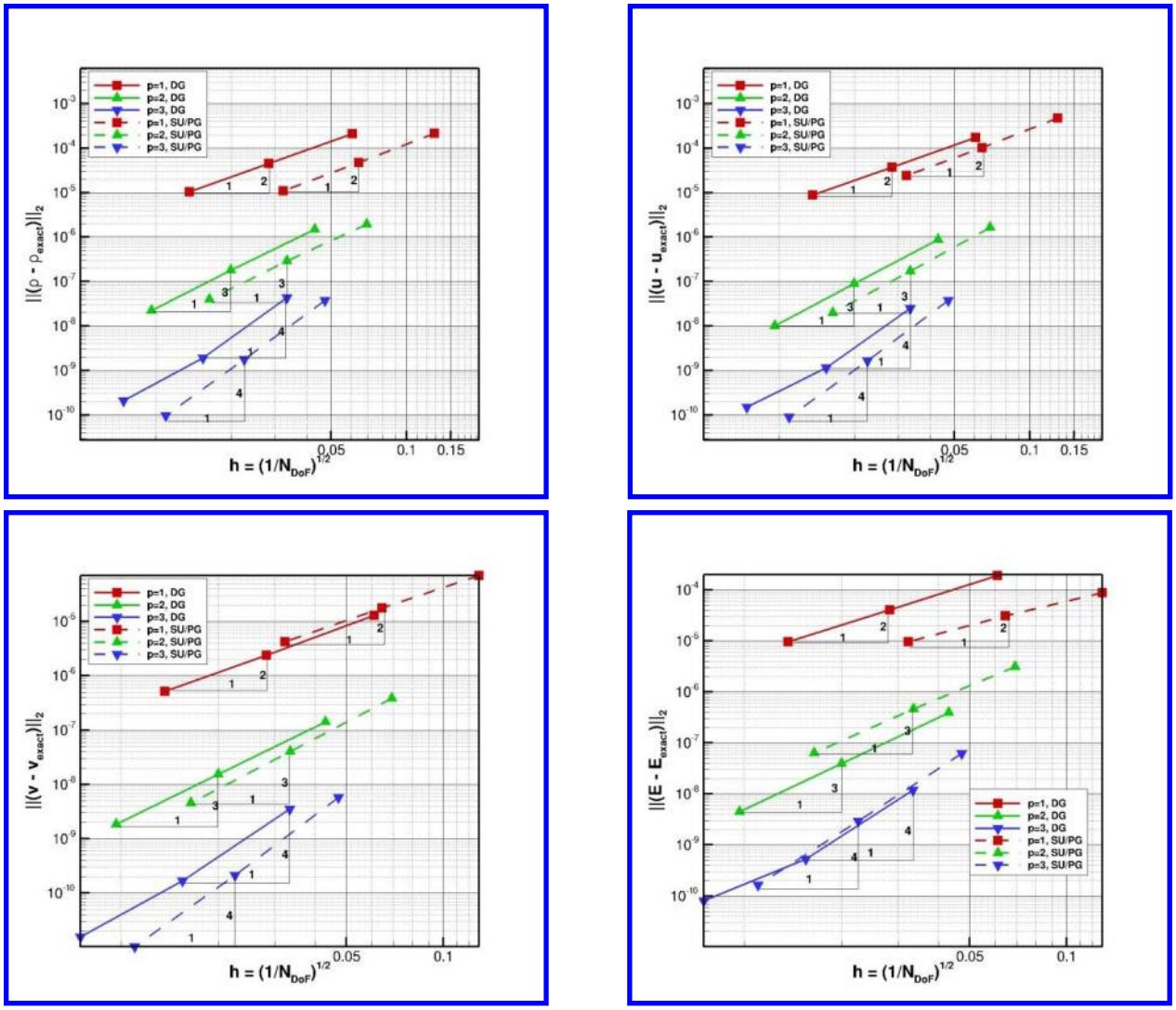

Figure 3. Comparison of the L_2 error norm vs. $\sqrt{1/N_{DoF}}$ for the SU/PG and DG methods at Re = 10 for method of manufactured solutions.

Fig. 4 compares error in density, velocity, and total energy vs. the number of elements (N_{Elmt}) in each mesh for the SU/PG and DG methods. Fig. 4 shows that on a given mesh the level of error is comparable for both FE methods at p = 1, 2, and 3.

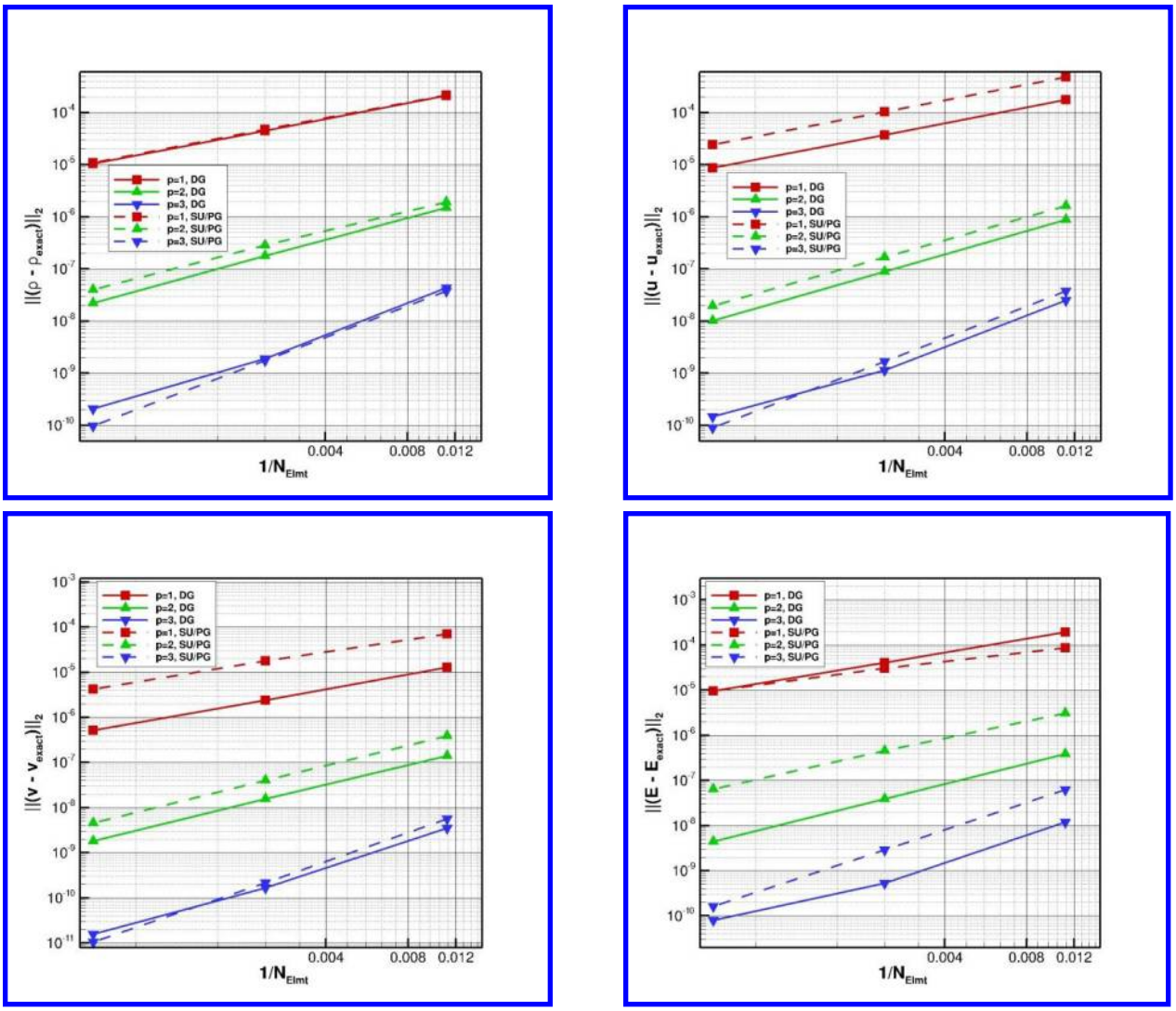

Figure 4. Comparison of the L_2 error norm vs. $1/N_{Elmt}$ for the SU/PG and DG methods at Re=10 for method of manufactured solutions.

Table 1 is a breakout of the data presented in Figs. 3 and 4 with the addition of the number of non-zero entries in the matrix system for each FE method on each grid at each p level. The number of non-zero entries in the matrix system is a rough measure of the work involved in inverting the matrix system. For the meshes utilized in this study at p = 1 the DG method has ~10 times more nonzero (N_{NZ}) entries, at p = 2 the DG method has ~6 times more nonzero entries, and at p = 3 the DG method has ~5 times more nonzero entries to the matrix system.

Table 1. Comparison of grid and matrix metrics for SU/PG and DG techniques for method of manufactured solutions.

a. 90 Elements

Order (P)	N_{DoF}	N_{NZ}	$\|\rho - \rho_{exact}\|_2$	$\|u - u_{exact}\|_2$	$\|v - v_{exact}\|_2$	$\|E - E_{exact}\|_2$
DG 1	270	3240	2.1041844E-4	1.7427689E-4	1.2802861E-5	1.9114469E-4
SU/PG 1	60	358	2.1578774E-4	4.7476862E-4	7.0044856E-5	8.7069725E-5
DG 2	540	12960	1.4902872E-6	8.7650590E-7	1.4187059E-7	3.8677042E-7
SU/PG 2	209	2183	1.9135246E-6	1.6286604E-6	3.8418864E-7	3.1097047E-6
DG 3	900	36000	4.3064904E-8	2.5067797E-8	3.5406886E-9	1.1947010E-8
SU/PG 3	448	7096	3.7692124E-8	3.7194980E-8	5.7117978E-9	6.2500787E-8

b. 418 Elements

Order (P)	N_{DoF}	N_{NZ}	$\|\rho - \rho_{exact}\|_2$	$\|u - u_{exact}\|_2$	$\|v - v_{exact}\|_2$	$\|E - E_{exact}\|_2$
DG 1	1254	15048	4.4941492E-5	3.7329989E-5	2.3917577E-6	4.0923215E-5
SU/PG 1	240	1554	4.7503233E-5	1.0333975E-4	1.7654636E-5	3.0568125E-5
DG 2	2508	60192	1.7729169E-7	8.8741424E-8	1.5483129E-8	3.9251549E-8
SU/PG 2	897	9855	2.8709335E-7	1.6887693E-7	4.0301236E-8	4.5934434E-7
DG 3	4180	167200	1.8965142E-9	1.1405213E-9	1.669977E-10	5.310525E-10
SU/PG 3	1972	32428	1.7578031E-9	1.6648038E-9	2.141679E-10	2.9330966E-9

c. 1794 Elements

Order (P)	N_{DoF}	N_{NZ}	$\|\rho - \rho_{exact}\|_2$	$\|u - u_{exact}\|_2$	$\|v - v_{exact}\|_2$	$\|E - E_{exact}\|_2$
DG 1	5382	64584	1.0441537E-5	8.6961671E-6	5.2012633E-7	9.5266343E-6
SU/PG 1	960	6466	1.0958612E-5	2.4378150E-5	4.1793215E-6	9.6427219E-6
DG 2	10764	258336	2.2235117E-8	1.0085325E-8	1.8257676E-9	4.4572374E-9
SU/PG 2	3713	41759	3.9743217E-8	1.9364769E-8	4.5314748E-9	6.3425261E-8
DG 3	17940	717600	2.092352E-10	1.472061E-10	1.559322E-11	7.978069E-11
SU/PG 3	8260	138172	9.652045E-11	8.889664E-11	1.042542E-11	1.618252E-10

B. NACA0012 Laminar Airfoil

The second test case is the simulation of the flow over a NACA0012 airfoil using both the SU/PG and DG FE methods. The flow conditions are Mach number = 0.5, $\alpha = 1^{\circ}$, Re = 5,000 (based on chord length), which results in a flow that is steady in the limit of infinite time. The airfoil surface is assumed to be an adiabatic no-slip wall, and subsonic flow characteristic in/out flow boundary conditions are specified at the far-field. Regardless of the discretization method employed, all results are shown at steady-state conditions and were obtained by solving the steady NS equations using a damped Newton's method. For this case, the mesh contains 9,214 triangular elements and discretization orders p = 1, 2, and 3 are employed. While every effort was made to minimize implementation differences between the two CFD solvers, the DG solver employs orders of p+1 for curved boundaries, and the SU/PG solver employs geometry orders of p.

Fig. 5 shows the computational mesh (the outer boundary is ~40 chord lengths away from airfoil) and the computed Mach number contours generated by both FE methods for p = 1, 2, and 3. For this case both SU/PG and DG methods produce similar qualitative results on the same mesh. In both cases p = 3 or cubic polynomials offer increased wake resolution compared with solutions generated with lower p.

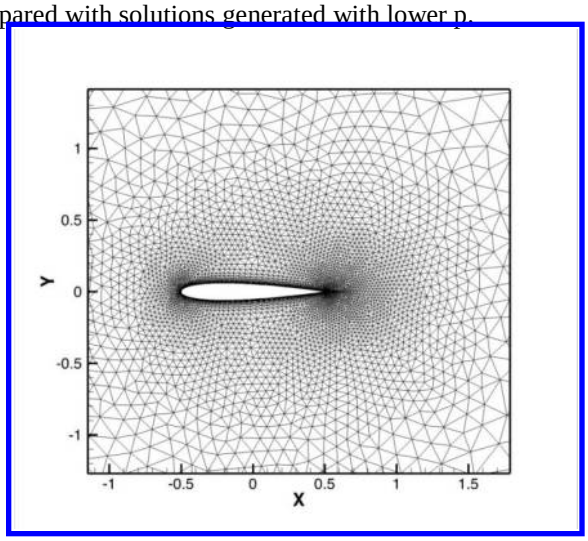

Initial Mesh, Linear Elements

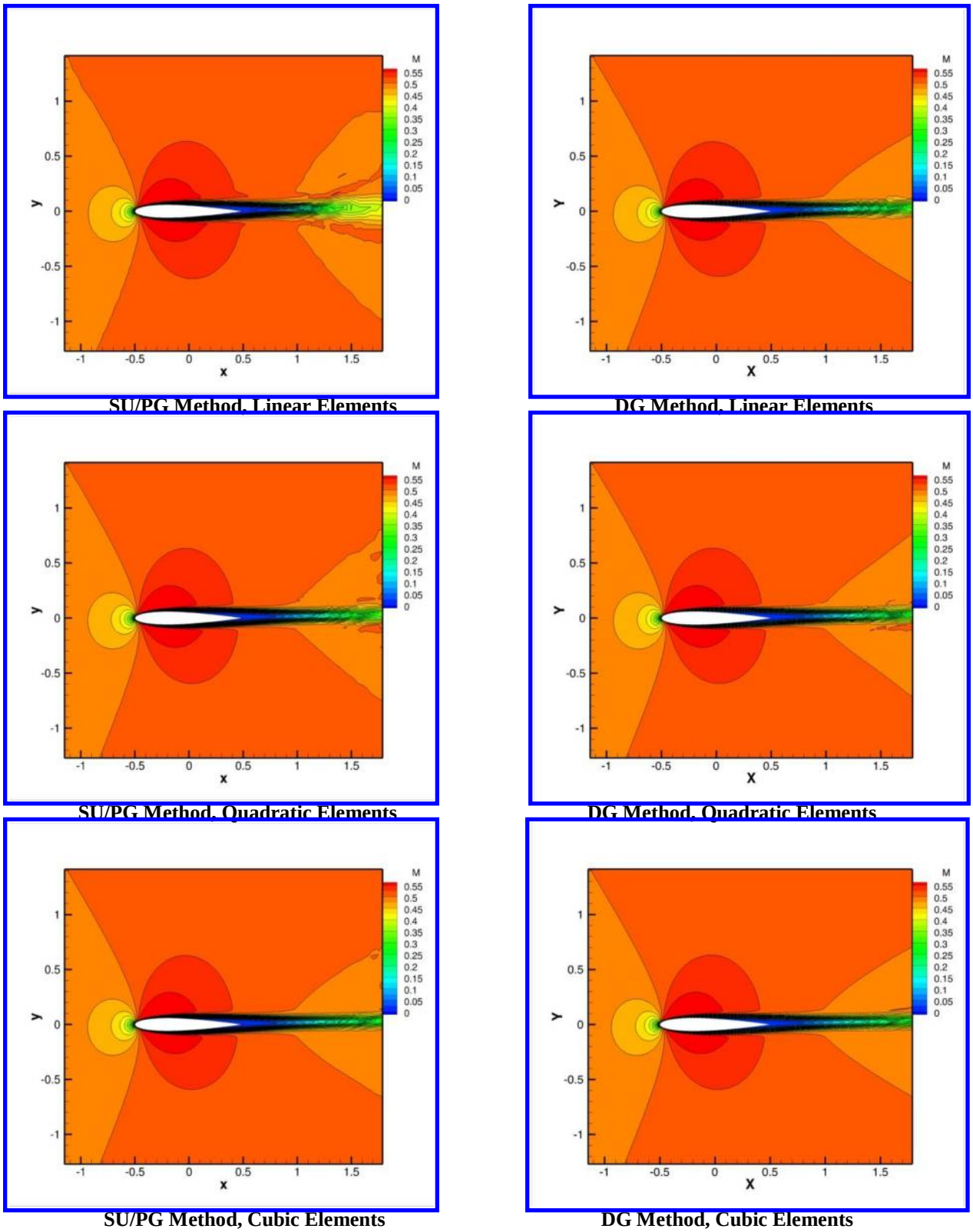

SU/PG Method, Linear Elements | DG Method, Linear Elements

SU/PG Method, Quadratic Elements | DG Method, Quadratic Elements

SU/PG Method, Cubic Elements | DG Method, Cubic Elements

Figure 5. Qualitative comparison of Mach number contours of the SU/PG and DG methods for flow over a NACA0012 airfoil at $\alpha = 1^{\circ}$, Re = 5,000, and Mach number = 0.5.

Table 2 contains the computed lift and drag coefficients obtained using the SU/PG and DG methods compared to reference quantities generated by the DG method on a mesh with 250,000 degrees of freedom and p = 4 elements employed. Table 2 shows that using the same mesh and discretization order SU/PG and DG methods obtain similar results for these simulation outputs. Recalling that FE methods literature is mainly made up of DG methods, it is encouraging to note that the SU/PG solver is generating results that very closely match a well- verified/validated DG solver.[3,7]

Table 2. Comparison of grid and matrix metrics for SU/PG and DG methods for flow over a NACA0012 airfoil at $\alpha = 1^{\circ}$, Re = 5,000 and Mach number = 0.5.

a. 9,214 Elements

Order (P)	N_{DoF}	N_{NZ}	C_L	$C_{L\ Ref}$	C_D	$C_{D\ Ref}$
DG 1	27642	331704	0.0242452	0.0184321	0.0549085	0.0559061
SU/PG 1	4689	32495	0.0149908	0.0184321	0.0548850	0.0559061
DG 2	55284	1326816	0.0196699	0.0184321	0.0561271	0.0559061
SU/PG 2	18592	212578	0.0191174	0.0184321	0.0550188	0.0559061
DG 3	92140	3685600	0.0192616	0.0184321	0.0560289	0.0559061
SU/PG 3	41709	706101	0.0186652	0.0184321	0.0551122	0.0559061

C. Low Speed Laminar Circular Cylinder

The third test case studies the unsteady flow over an impulsively started circular cylinder using both the SU/PG and DG FE methods. The flow conditions are Mach number = 0.2, $\alpha = 0^{\circ}$, Re = 40 (based on cylinder diameter), which results in unsteady laminar flow. For each FE method second-order backward differencing with a constant nondimensional time-step $\left(\Delta t^* = \frac{\Delta t a_\infty}{D}\right)$ of 0.05 is employed along with Newton's method to march the solution forward in time. Both the SU/PG and DG solvers drive the residual to machine zero at each time step through the usage of subiterations. The cylinder surface is assumed to be an adiabatic no-slip wall, and subsonic flow characteristic in/out flow boundary conditions are specified at the far-field. For this case the mesh contains 9,355 elements, and discretization orders p = 1, 2, and 3 are employed.

Fig. 6 shows the computational mesh (the outer boundary is ~20 diameters away from the cylinder) and the computed Mach number contours generated by both methods for p = 1, 2, and 3 at nondimensional time based on free-stream velocity $\left(\frac{tu_\infty}{D}\right)$ = 10.5. As with the NACA0012 case, for the cylinder case both FE methods produce similar qualitative results on the same mesh, and wake resolution is increased with higher p.

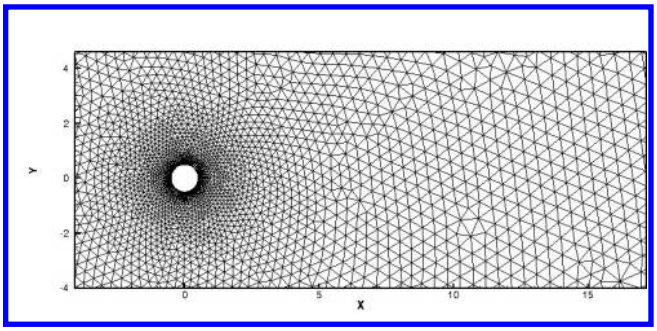

Initial Mesh, Linear Elements

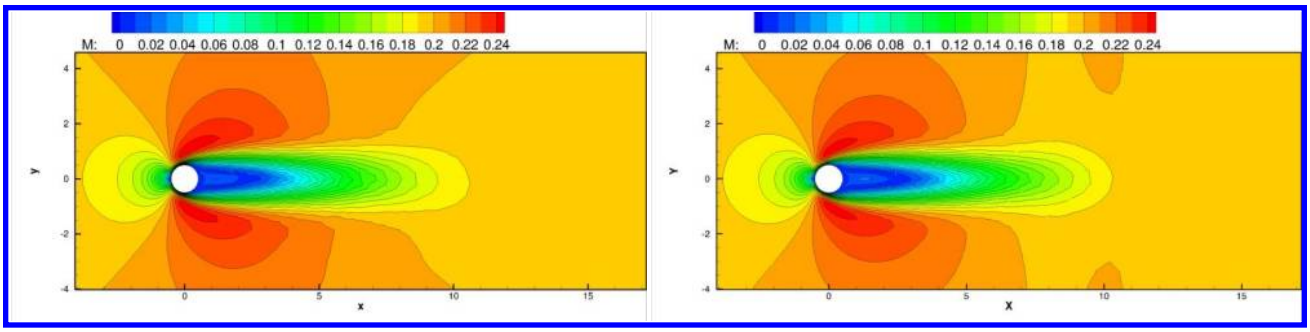

SU/PG Method, Linear Elements **DG Method, Linear Elements**

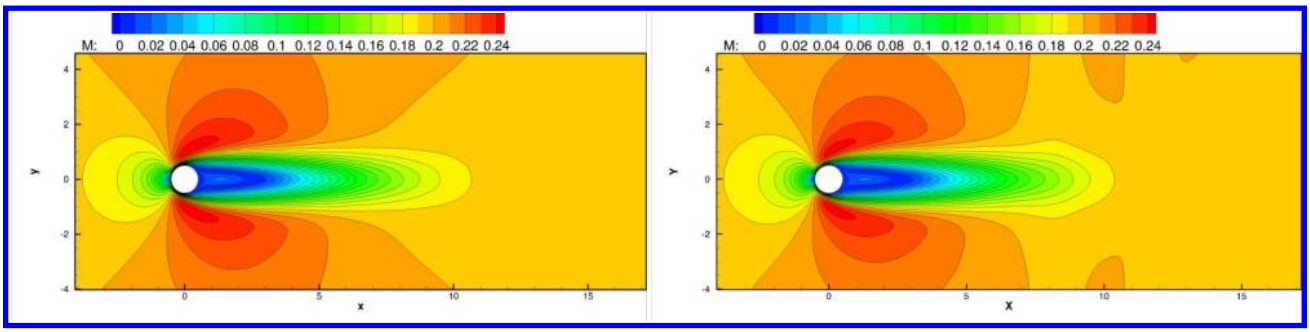

SU/PG Method, Quadratic Elements **DG Method, Quadratic Elements**

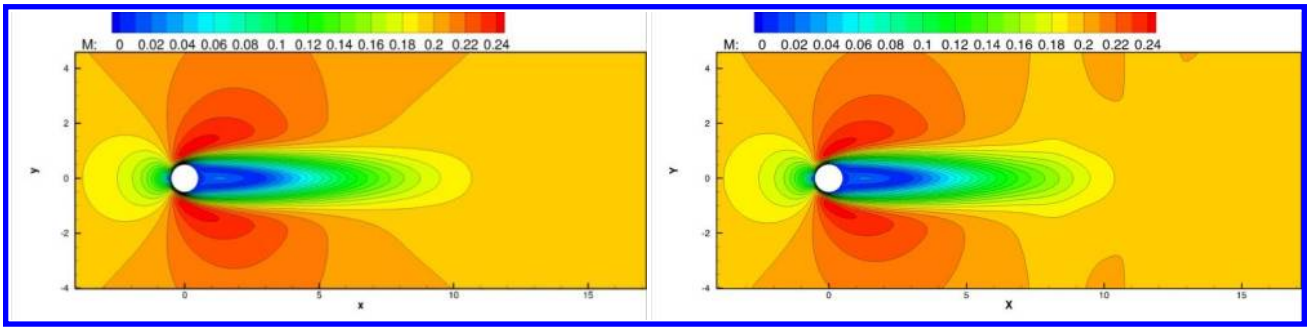

SU/PG Method, Cubic Methods **DG Method, Cubic Elements**

Figure 6. Qualitative comparison of Mach number contours of the SU/PG and DG methods for flow over a 2D cylinder at Re = 40, Mach number = 0.2, Time = 10.5.

Fig. 7 shows the computed solution from the SU/PG and DG methods compared to an experimental solution[21, 22] at nondimensional time equals 2.7, 3.7, 5.3, and 10.5. For this mesh both CFD solvers show good agreement with the experimental data at each time and p level.

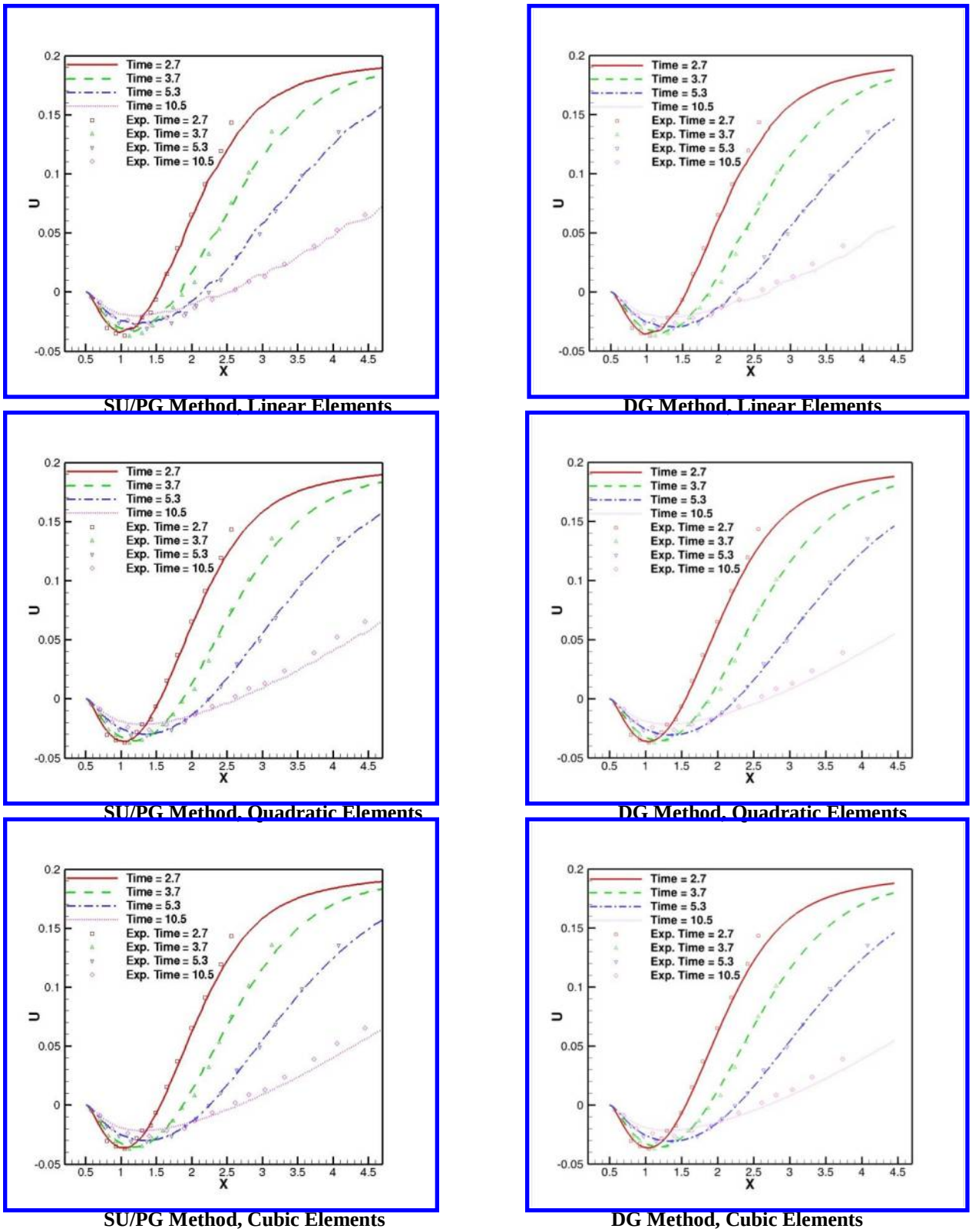

Figure 7. Comparison of SU/PG and DG methods with experimentally generated data.

Table 3 contains the computed lift and drag coefficients obtained using the SU/PG and DG methods at nondimensional time = 10.5 as compared to reference quantities.[23] Table 3 shows that for this unsteady problem, the SU/PG and DG methods compute similar force coefficients for p = 1, 2, and 3. Table 3 also shows that the number of degrees of freedom and the number of nonzero entries in the matrix system are significantly fewer for the SU/PG method.

Table 3. Comparison of grid and matrix metrics for SU/PG and DG methods for cylinder.

a. 9,355 Elements

Order (P)	N_{DoF}	N_{NZ}	C_L (T=10.5)	C_L^{Ref}	C_D (T=10.5)	C_D^{Ref}
DG 1	28065	331704	0.019940008	0	1.705180	~1.65
SU/PG 1	4809	33137	0.033484060	0	1.659555	~1.65
DG 2	56130	1326816	0.001166707	0	1.646849	~1.65
SU/PG 2	18973	216217	0.005346940	0	1.660706	~1.65
DG 3	93550	3685600	-0.000079718	0	1.644808	~1.65
SU/PG 3	42492	717630	0.004346445	0	1.663870	~1.65

V. Conclusion

These test cases demonstrate that SU/PG and DG FE methods give comparable qualitative and quantitative results using the same meshes for various real-world flow problems. The SU/PG method employs fewer degrees of freedom and has fewer nonzero entries in its matrix system at the p levels tested than the DG method. For the levels of p examined in this paper, both the SU/PG and DG methods are viable finite-element discretization methods. In the future, both of these methods will be implemented in three spatial dimensions in the same code, which will eliminate implementation differences between the two methods so that valid wall-clock time measurements can be made for an array of test cases. Further testing will be performed with this unified code on three-dimensional steady and unsteady flow cases covering a wide range of flow speeds including cases with shocks and turbulent flow. Since both FE methods give comparable results on identical meshes, wall-clock time is an appropriate quantity to compare. However, due to the differences in implementation this is left for future research.

References

[1]Venkatakrishnan, V., Allmaras, S. R., Kamenetskii, D. S., and Johnson, F. T., "Higher Order Schemes for the Compressible Navier-Stokes Equations," *16th AIAA Computational Fluid Dynamics Conference*, Orlando, FL, June 2003, AIAA 2003-3987.

[2]Erwin, J. T., Anderson, W. K., Kapadia, S., Wang, L., "Three Dimensional Stabilized Finite Elements for Compressible Navier-Stokes," *20th AIAA Computational Fluid Dynamics Conference*, Honolulu, HI, June 2011, AIAA 2011-3411.

[3]Burgess, N. K., Nastase, C. R., Mavriplis, D. J., "Efficient Solution Techniques for Discontinuous Galerkin Discretizations of the Navier-Stokes Equations on Hybrid Anisotropic Meshes," *48th AIAA Aerospace Sciences Meeting*, Orlando, FL, January 2010, AIAA 2010-1448.

[4]Kirk, B. S. and Carey, G. F., "Development and Validation of a SUPG Finite Element Scheme for the Compressible Navier-Stokes Equations Using a Modified Inviscid Flux Discretization," *International Journal for Numerical Methods in Fluids*, Vol. 57, No. 3, 2008, pp. 265-293.

[5]Kirk, B. S., Bova, S. W., and Bond, R. B., "The Influence of Stabilization Parameters in the SUPG Finite Element Method for Hypersonic Flows," *48th AIAA Aerospace Sciences Meeting*, Orlando, FL, January 2010, AIAA 2010-1183.

[6]Wang, L., *Techniques for High-order Adaptive Discontinuous Galerkin Discretizations in Fluid Dynamics*, Ph. D. thesis, University of Wyoming, April 2009.

[7]Burgess, N. K., *An Adaptive Discontinuous Galerkin Solver for Aerodynamic Flows*, Ph. D. thesis, University of Wyoming, November 2011.

[8]Bonhaus, D. L., *A Higher Order Accurate Finite Element Method for Viscous Compressible Flows*, Ph. D. thesis, Virginia Polytechnic Institute and State University, November 1998.

[9]Brooks, A. N. and Hughes, T. J. R., "Streamline Upwind/Petrov-Galerkin Formulations for Convection Dominated Flows with Particular Emphasis on the Incompressible Navier-Stokes Equations," *Computer Methods in Applied Mechanics and Engineering*, Vol. 32, No. 1-3, September 1982, pp. 199-259.

[10]Saad, Y. and Schultz, M. H., "GMRES: A Generalized Minimal Residual Algorithm for Solving Nonsymmetric Linear Systems," *SIAM J. Sci. Stat. Comput.*, Vol. 7, No. 3, 1986, pp. 856-869.

[11]Barth, T. J., "Numerical Methods for Gasdynamic Systems on Unstructured Meshes," *An Introduction to Recent Developments in Theory and Numerics for Conservation Laws*, edited by D. Kroner, M. Ohlberger, and C. Rhode, Vol. 5, Springer, New York, NY, 1998, pp. 195-285.

[12]Shakib, F., Hughes, T. J., and Johan, Z., "A New Finite Element Formulation for Computational Fluid Dynamics: X. The Compressible Euler and Navier-Stokes Equations," *Computer Methods in Applied Mechanics and Engineering*, Vol. 89, No. 1-3, 1991, pp. 141-219, Second World Congress on Computational Mechanics.

[13]Davis, S. F., "Simplified Second-Order Godunov-Type Methods," *SIAM J. Sci. Stat. Comput.*, Vol. 9, No. 3, 1988, pp. 445-473.

[14]Roe, P. L., "Approximate Riemann Solvers, Parameter Vectors, and Difference Schemes," *J. Comput. Phys.*, Vol. 43, 1981, pp. 357-372.

[15]Harten, A., Lax, P. D., and Van Leer, B., "On Upstream Differencing and Godunov-Type Schemes for Hyperbolic Conservations Laws," *Siam Review*, Vol. 25, No. 1, 1983, pp. 35-61.

[16]Toro, F. E., *Riemann Solvers and Numerical Methods for Fluid Dynamics*, Applied Mechanics, Springer-Verlag, New York, NY, 1999.

[17]Batten, P., Clarke, N., Lambert, C., and Causon, D. M., "On the Choice of Wavespeeds for the HLLC Riemann Solver," *SIAM J. Sci. Comput.*, Vol. 18, No. 2, 1997, pp. 1553-1570.

[18]Batten, P., Leschiner, M. A., and Goldberg, U. C., "Average-State Jacobians and Implicit Methods for Compressible Viscous and Turbulent Flows," *J. Comput. Phys.*, Vol. 137, 1997, pp. 38-78.

[19]Shahbazi, K., *A Parallel High-Order Discontinuous Galerkin Solver for the Unsteady Incompressible Navier-Stokes Equations in Complex Geometries*, Ph. D. thesis, University of Toronto, May 2007.

[20]Hartmann, R. and Houston, P., "Symmetric Interior Penalty DG Methods for Compressible Navier-Stokes Equations I: Method Formulation," *Internal Journal of Numerical Analysis and Modeling*, Vol. 3, No. 1, 2006, pp. 1-20.

[21]Coutanceau, M. and Bouard, R., "Experimental Determination of the Main Features of the Viscous Flow in the Wake of a Circular Cylinder in Uniform Translation. Part 1. Steady flow," *Journal of Fluid Mechanics*, Vol. 79, No. 02, 1977, pp. 231-256.

[22]Coutanceau, M. and Bouard, R., "Experimental Determination of the Main Features of the Viscous Flow in the Wake of a Circular Cylinder in Uniform Translation. Part 2. Unsteady flow," *Journal of Fluid Mechanics*, Vol. 79, No. 02, 1977, pp. 257-272.

[23]Lindsey, W. F., "Drag of Cylinders of Simple Shapes," *National Advisory Committee for Aeronautics*, Report No. 619, 1937, pp. 169-176.